

Models of Microbial Dormancy in Biofilms and Planktonic Cultures

Bruce P. Ayati* Isaac Klapper†

September 18, 2018

Abstract

We present models of dormancy in a planktonic culture and in biofilm, and examine the relative advantage of short dormancy versus long dormancy times in each case. Simulations and analyses indicate that in planktonic batch cultures and in chemostats, live biomass is maximized by the fastest possible exit from dormancy. The lower limit of time to reawakening is thus perhaps governed by physiological, biochemical or other constraints within the cells. In biofilm we see that the slower waker has a defensive advantage over the fast waker due to a larger amount of dormant biomass, without an appreciable difference in total live biomass. Thus it would seem that typical laboratory culture conditions can be unrepresentative of the natural state. We discuss the computational methods developed for this work.

1 Introduction

Microbial populations, particularly those in biofilms (sessile, matrix encased communities, see [11] for an overview), can contain cells in varying phenotypic states. An important difference between planktonic (free-swimming) and biofilm environments is that the former is generally well-mixed whereas the latter is unmixed and spatially heterogeneous as a result. As a result of their self-generated spatially variable environmental, biofilms demonstrate spatially diverse ecology [20, 17]. Such diversification may be advantageous for defense against an uncertain and temporally varying environment. For example, though cell states that are more tolerant to antimicrobial challenge may be less competitive in the

*Department of Mathematics and Program in Applied Mathematical & Computational Sciences, University of Iowa, Iowa City, IA 52242-1419 (bruce-ayati@uiowa.edu). This material is based upon work supported by the National Science Foundation under Grant No. DMS-0914514.

†Department of Mathematical Sciences and Center for Biofilm Engineering, Montana State University (klapper@math.montana.edu). This material is based upon work supported by the National Science Foundation under Grant Nos. DMS-0934696 and DMS-0826975.

absence of that challenge, their presence can improve community survivability against attack.

Here we consider one such defense mechanism, dormancy (possibly related to the phenomenon of persister cells [5, 12]) where, in response to an environmental stress, cells differentiate into a protected, slow- or non-growing condition [7, 15]. Bacteria in planktonic states have been found to revive faster from dormancy than those in a biofilm state [7]. Thus it would seem that dormancy-regulating parameters are subject to influence of environmental variation, at least of the sort found in biofilms. Here we wish to use modeling tools in order to gain insight into role and regulation of dormancy in spatially mixed systems (batch and chemostat microbial communities) and unmixed systems (biofilm communities). Our attention is directed to the relative advantage of short dormancy versus long dormancy times in the cases of batch, chemostat, and biofilm states.

In the process, we also present computational tools designed to study dormancy within batch, chemostat, and biofilm population dynamics, in particular with respect to competitiveness. These tools are an extension of those discussed in [5] for persistence and senescence, primarily in the numerical methods used to solve the more general physiological structure used in this paper, and we expect they will have wider applicability to descriptions of physiological states in both mixed and unmixed microbial communities. The physiological structure is represented by a continuous variable. Compartmentalized dormancy models have been considered elsewhere [13, 14].

This paper is organized as follows. We present models of chemostat and batch cultures, and asymptotic analyses of their long-time behavior. We then derive the biofilm model. We compute numerical solutions of the model equations for the batch, chemostat and biofilm cultures, and discuss the numerical methods developed for these computations. We conclude with the implications of our results.

2 Models of Dormancy in Chemostat and Batch Cultures

We introduce $s \in [s_0, s^*]$ to index the dormancy state of individual cells, with s_0 the value at which cells enter dormancy and s^* the value at which cells leave dormancy and become active. Cells progress through dormancy states with “speed” $g(s, c)$, where c is concentration of relevant chemicals (e.g. substrates or antimicrobials); for example, large concentrations of substrates and/or small concentrations of antimicrobials imply larger value of g . While dormant, cells do not grow and divide; on the other hand, dormant cells are presumed to be harder in response to environmental stress.

Let $t \geq 0$ represent time. Let $u(t)$ represent the density of active cells, $v(s, t)$ represent the density of dormant cells, and $c(t)$ be a vector of substrate chemical species concentrations. Let the operator ∂_y denote partial differentiation in the subscript variable y . The active cell population is modeled by an ordinary

differential equation, $t > 0$,

$$\frac{d}{dt}u(t) = \underbrace{b(c)u(t)}_{\text{cell division}} - \underbrace{\mu_u(c)u(t)}_{\text{death}} + \underbrace{g(s^*, c)v(s^*, t)}_{\text{exit from dormancy}} - \underbrace{h(c)u(t)}_{\text{entrance to dormancy}} - \underbrace{d_0u(t)}_{\text{washout}}, \quad (1a)$$

where d_0 is the chemostat dilution rate (roughly, inverse of the time scale for the chemostat contents to be flushed). The functions b and μ_u account for cell division and cell “death”. We use “death” as shorthand for all forms of inertness not tied to strategic dormancy on the part of the bacteria. The function $h \geq 0$ is the dormancy rate of active cells. Let $g \geq 0$ (as above) and $\mu_v > 0$ denote the reactivation and death rates, resp., of the dormant cells. We use a physiologically structured equation for the dormant cell population,

$$\partial_t v(s, t) + \underbrace{\partial_s(g(s, c)v(s, t))}_{\text{reactivation kinetics}} = \underbrace{-\mu_v(s, c)v(s, t)}_{\text{death}} - \underbrace{d_0v(s, t)}_{\text{washout}}, \quad (1b)$$

$$g(s_0, c)v(s_0, t) = \underbrace{h(c)u(t)}_{\text{creation of newly dormant cells}}, \quad (1c)$$

for $s_0 < s \leq s^*$. For the substrate chemicals, we have

$$\frac{d}{dt}c(t) = -\underbrace{f(c(t), u(t), v(\cdot, t))}_{\text{chemical reactions}} + \underbrace{d_0(C_0(t) - c(t))}_{\text{chemostat turnover}}, \quad (1d)$$

where f is the vector of reactions and $C_0(t)$ is the input concentration vector from the chemostat tank. Initial conditions are $u(0) = u_0$, $v(0, s) = v_0(s)$, and $c(0) = c_0$. The model for a batch culture is obtained from (1) by setting $d_0 = 0$.

3 Long-Time Behavior

In this section we examine the long-time behavior of chemostat models for steady and periodic cases.

3.1 Steady Chemostat

We consider the long-time behavior of the steady ($C_0(t) = C_0$) chemostat system by studying the time-independent solution of equations (1). In the steady state $c(t) = c$, so that we can define a new dormancy coordinate $a \in [0, a^*]$ by

$$a(s) = \int_{s_0}^s \frac{ds'}{g(s', c)}, \quad (2)$$

with $a^* = a(s^*)$. Setting the time derivative to zero, (1b) together with (1c) can be solved to obtain

$$v(a) = \frac{h(c)u}{g(a^*, c)} e^{-d_0 a} e^{-\int_0^a \mu_v(a', c) da'}, \quad (3)$$

where u is the steady state value of the active cell density and s has been replaced by a . The first exponential factor accounts for loss due to washout and the second for loss due to death. Plugging into (1a) and again setting the time-derivative to zero, we obtain

$$0 = u \left[b(c) - \mu_u(c) - d_0 - \left(1 - e^{-d_0 a^*} e^{-\int_0^{a^*} \mu_v(a,c) da} \right) h(c) \right]. \quad (4)$$

If $u \neq 0$, then the second factor of (4) provides an equation for c . Assuming that μ_u , μ_v , and h are all decreasing functions of c , we can write that second factor in the form $b(c) - \bar{\alpha} - \tilde{\alpha}(c)$, where $\bar{\alpha}$ is a constant and $\tilde{\alpha}(c)$ is a decreasing function of c such that $\tilde{\alpha}(c) \rightarrow 0$ as $c \rightarrow \infty$. Thus, assuming that $b(c)$ is a monotone increasing function of c and that $b(c) > \bar{\alpha}$ for c sufficiently large, then it follows that there is a unique value of c that solves (4) with $u \neq 0$. However if that value is larger than C_0 or if $b(c) < \bar{\alpha}$ for all c , then the only admissible solution of (4) is $u = 0$ (washout).

Finally, given the solution for c , equation (1d) can be solved to obtain the long-time behavior of u by setting the time derivative to zero¹. In the case that f is monotone increasing in its arguments, we obtain a unique solution for u .

For two (or more) species competing in the same chemostat, the one that has the steady-state solution with smallest value of substrate c is the only long-time survivor [16]; it excludes the other species by continually reducing substrate until substrate level is below the others' steady-state requirements. Thus, from (4) it is apparent that the smaller the size of h (i.e., the lesser the likelihood of entry to dormancy) and the smaller the value of a^* (i.e., the shorter the dormancy period), the more competitive the species. Note that a species which does not go dormant at all will outcompete an otherwise similar species which does.

3.2 Periodic Chemostat

We consider next the long-time behavior of a periodic chemostat with input substrate concentration $C_0(\omega t)$ where $C_0(a+1) = C_0(a)$, and offer asymptotics for two special cases.

3.2.1 Fast Oscillations

We suppose that the chemostat oscillation period is short compared to all other time scales of interest. In this limit, the chemostat will oscillate many times before the microbial inhabitants can react. This intuition suggests a multiple time scale expansion with a slow time t_1 and a fast time t_2 defined by

$$t_1 = t, \quad t_2 = \epsilon^{-1}t, \quad (5)$$

¹If $u = 0$, then (1d) requires that $d_0(C_0 - c) = f(c, 0, 0)$; generally $f(c, 0, 0) = 0$ in which case $c = C_0$.

where $\epsilon = \omega^{-1} \ll \tau$ for any inherent time scale τ in the system. Note $C_0 = C_0(t_2)$. We expand

$$u = u_0(t_1, t_2) + \epsilon u_1(t_1, t_2) + \dots, \quad (6a)$$

$$v = v_0(s, t_1, t_2) + \epsilon v_1(s, t_1, t_2) + \dots, \quad (6b)$$

$$c = c_0(t_1, t_2) + \epsilon c_1(t_1, t_2) + \dots, \quad (6c)$$

We suppose that the solution (u, v, c) approaches periodicity with period ω^{-1} for long times, so we look for a solution independent of slow time t_1 , i.e.,

$$u = u_0(t_2) + \epsilon u_1(t_2) + \dots, \quad (7a)$$

$$v = v_0(s, t_2) + \epsilon v_1(s, t_2) + \dots, \quad (7b)$$

$$c = c_0(t_2) + \epsilon c_1(t_2) + \dots, \quad (7c)$$

In this case, $d/dt = \epsilon^{-1}d/dt_2$. Then to lowest order ($= O(\epsilon^{-1})$), system (1) becomes

$$\frac{\partial u_0}{\partial t_2} = \frac{\partial v_0}{\partial t_2} = \frac{\partial c_0}{\partial t_2} = 0, \quad (8)$$

so that u_0, c_0 are constants and $v_0 = v_0(s)$, i.e.,

$$u = u_0 + \epsilon u_1(t_2) + \dots, \quad (9a)$$

$$v = v_0(s) + \epsilon v_1(s, t_2) + \dots, \quad (9b)$$

$$c = c_0 + \epsilon c_1(t_2) + \dots, \quad (9c)$$

At the next order ($= O(\epsilon^0)$), system (1) becomes

$$\frac{d}{dt_2} u_1(t_2) = b(c_0)u_0 - \mu_u(c_0)u_0 + g(s^*, c_0)v_0(s^*) - h(c_0)u_0 - d_0u_0, \quad (10a)$$

$$\frac{\partial}{\partial t_2} v_1(s, t_2) = -\partial_s(g(s, c_0)v_0(s)) - \mu_v(s, c_0)v_0(s) - d_0v_0(s), \quad (10b)$$

$$\frac{\partial}{\partial t_2} c_1(t_2) = -f(c_0, u_0, v_0(\cdot)) + d_0(C_0(t_2) - c_0), \quad (10c)$$

with $g(s_0, c_0)v(s_0) = h(c_0)u_0$. Averaging over a period ω^{-1} , we obtain

$$0 = b(c_0)u_0 - \mu_u(c_0)u_0 + g(s^*, c_0)v_0(s^*) - h(c_0)u_0 - d_0u_0, \quad (11)$$

$$0 = -\partial_s(g(s, c_0)v_0(s)) - \mu_v(s, c_0)v_0(s) - d_0v_0(s), \quad (12)$$

$$0 = -f(c_0, u_0, v_0(\cdot)) + d_0(\bar{C}_0 - c_0), \quad (13)$$

with $g(s_0, c_0)v(s_0) = h(c_0)u_0$, where \bar{C}_0 is the average of $C_0(t_2)$ over one chemostat oscillation period. This system, the same as was solved previously in the steady chemostat case except with \bar{C}_0 replacing C_0 , has essentially the same solutions for $u_0, v_0(s)$, and c_0 ; the next order terms $u_1(t_2), v_1(s, t_2), c_1(t_2)$ add a correction of $O(\epsilon)$. Note thus that the same conclusion holds: a species without dormancy will outcompete an otherwise similar species which can go dormant (because the fast oscillating chemostat acts like a steady chemostat with input substrate \bar{C}_0).

3.2.2 Slow Oscillations

We suppose now that the chemostat oscillation period is long compared to all other time scales of interest, i.e., that the chemostat can nearly reach equilibrium before input $C_0(\omega t)$ changes noticeably. Intuition again suggests a multiple time scale expansion with a slow time t_1 and a fast time t_2 , in this case defined by

$$t_1 = \epsilon t, \quad t_2 = t, \quad (14)$$

where $\epsilon = \omega \ll \tau^{-1}$ for any inherent time scale τ in the system. Note that $C_0 = C_0(t_1)$. We expand

$$u = u_0(t_1, t_2) + \epsilon u_1(t_1, t_2) + \dots, \quad (15a)$$

$$v = v_0(s, t_1, t_2) + \epsilon v_1(s, t_1, t_2) + \dots, \quad (15b)$$

$$c = c_0(t_1, t_2) + \epsilon c_1(t_1, t_2) + \dots, \quad (15c)$$

We suppose quasi-equilibrium in the sense that u_0 , v_0 , and c_0 are independent of fast time t_2 . Noting that $d/dt = \epsilon \partial/\partial t_1 + \partial/\partial t_2$, then at its slowest, ϵ^0 order, system (1) becomes

$$0 = b(c_0)u_0 - \mu_u(c_0)u_0 + g(s^*, c_0)v_0(s^*) - h(c_0)u_0 - d_0u_0, \quad (16a)$$

$$0 = -\partial_s(g(s, c_0)v_0) - \mu_v(s, c_0)v_0 - d_0v_0, \quad (16b)$$

$$0 = -f(c_0, u_0, v_0(\cdot)) + d_0(C_0(t_1) - c_0), \quad (16c)$$

with $g(s_0, c_0)v(s_0) = h(c_0)u_0$. Note that t_1 is essentially a parameter, appearing explicitly only in the input substrate concentration $C_0(t_1)$. Thus to zeroth order, the quantities u , v , and c obey system (16), which is the same as the steady chemostat except with parameterized input substrate. Hence we again conclude that a species that does not go dormant will outcompete an otherwise similar one that does. Note one caveat though: if $C(t_1)$ drops below the minimum required to sustain a particular population (see Section 3.1) at any point in its cycle, then extinction may occur.

4 A Model of Dormancy in a Biofilm

For the biofilm model we remove the chemostat-specific terms and extend the system (1) to include a spatial domain Ω consisting of stratified subdomains B_t for biomass and $\Omega \setminus B_t$ for the bulk fluid. There are two moving interfaces in Ω : Γ_t separating B_t from the rest of Ω , and a bulk-substrate interface Γ_{H_b} that is a fixed height H_b above Γ_t . The biofilm rests on a surface, denoted by a lower boundary, Γ_B . The spatial domains are illustrated in Figure 1. The active and dormant cell populations, and the chemical concentrations, now depend on $\mathbf{x} \in \Omega$. Conservation of biomass yields, for $t > 0$ and $s_0 < s \leq s^*$,

$$\begin{aligned} \partial_t u(\mathbf{x}, t) + \nabla \cdot \mathbf{J}_u = \\ b(c)u(\mathbf{x}, t) - \mu_u(c)u(\mathbf{x}, t) + g(s^*, c)v(\mathbf{x}, s^*, t) - h(c)u(\mathbf{x}, t), \end{aligned} \quad (17a)$$

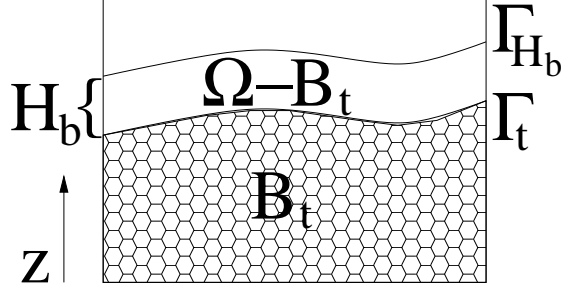


Figure 1: Spatial domains for the biofilm model.

$$\partial_t v(\mathbf{x}, s, t) + \partial_s(g(s, c)v(\mathbf{x}, s, t)) + \nabla \cdot \mathbf{J}_v = -\mu_v(s, c)v(\mathbf{x}, s, t), \quad (17b)$$

$$g(s_0, c)v(\mathbf{x}, s_0, t) = h(c)u(\mathbf{x}, t), \quad (17c)$$

$$\partial_t w(\mathbf{x}, t) + \nabla \cdot \mathbf{J}_w = \mu_u(c)u(\mathbf{x}, t) + \int_{s_0}^{s^*} \mu_v(s, c)v(\mathbf{x}, s, t) ds, \quad (17d)$$

$$\partial_t c(\mathbf{x}, t) + \nabla \cdot \mathbf{J}_c = f(c(t), u(\mathbf{x}, t), v(\mathbf{x}, \cdot, t)), \quad (17e)$$

$$(17f)$$

where $\nabla \cdot$ denotes divergence in space, \mathbf{J}_y denotes the flux of subscript variable y , and where we assume appropriate initial conditions and boundary condition on the spatial domains.

Assuming Fick's Law gives $\mathbf{J}_c = -D\nabla c$ for diffusion constant D . The substrate masses are also subject to advection, but the velocity is sufficiently slow that we can neglect the advective contribution to the flux. Likewise, substrate material diffusion time scales are at least several orders of magnitude larger than the those at which bacteria grow or advect, allowing us to make a quasi-steady-state assumption so that

$$-D\nabla^2 c = f. \quad (18)$$

Let $\vartheta(\mathbf{x}, s, t)$ and $\rho(\mathbf{x}, s, t)$ denote the volume fraction per dormancy state and density per dormancy state relative to volume fraction, resp., of dormant cells. We assume incompressibility of biomass with $\rho(\mathbf{x}, s, t) \equiv \rho^*$ for positive constant ρ^* . We also assume, based on the fact that the main constituent of all cells is water, that active and inert cells have the same incompressibility properties, and the same densities relative to volume fractions, ρ^* , as dormant cells. We let $\nu(\mathbf{x}, t)$ and $\eta(\mathbf{x}, t)$ denote the volume fractions of active and dead cells, resp., which are related to the density of active and dead cells by $u = \rho^*\nu$ and $w = \rho^*\eta$.

Assume the biofilm polymer matrix exists in proportion to cell density. We require the biomass volume fractions to total to one so that

$$\nu(\mathbf{x}, t) + \eta(\mathbf{x}, t) + \int_{s_0}^{s^*} \vartheta(\mathbf{x}, s, t) ds = 1. \quad (19)$$

Assuming that transport of biomass, including dormant cells, is governed by an advective process, with a volumetric flow $\mathbf{u}(\mathbf{x}, t)$ for all classes and ages, gives the fluxes $\mathbf{J}_u = \rho^* u \mathbf{u}$, $\mathbf{J}_v = \rho^* v \mathbf{u}$ and $\mathbf{J}_w = \rho^* w \mathbf{u}$. As in [5], we follow [1, 10] and assume that the volumetric flow is stress driven according to

$$\mathbf{u} = -\lambda \nabla p, \quad (20)$$

where $p(t, \mathbf{x})$ is the pressure, $\lambda > 0$ the Darcy constant, and $p = 0$ in $\Omega \setminus B_t$. Pressure is determined in order to enforce incompressibility in response to growth and hence (20) can be viewed as a balance of growth-induced stress against friction. Other choices of force balance are possible.

Substituting $u = \rho^* \nu$, $\mathbf{J}_u = \rho^* u \mathbf{u}$, $v = \rho^* \vartheta$, $\mathbf{J}_v = \rho^* v \mathbf{u}$, $w = \rho^* \eta$, and $\mathbf{J}_w = \rho^* w \mathbf{u}$ into equations (17) gives

$$\begin{aligned} \partial_t \nu(\mathbf{x}, t) + \nabla \cdot (\mathbf{u} \nu) = \\ b(c) \nu(\mathbf{x}, t) - \mu_v(c) \nu(\mathbf{x}, t) + g(s^*, c) \vartheta(\mathbf{x}, s^*, t) - h(c) \nu(\mathbf{x}, t), \end{aligned} \quad (21a)$$

$$\partial_t \vartheta(\mathbf{x}, s, t) + \partial_s (g(s, c) \vartheta(\mathbf{x}, s, t)) + \nabla \cdot (\mathbf{u} \vartheta) = -\mu_v(s, c) \vartheta(\mathbf{x}, s, t), \quad (21b)$$

$$g(s_0, c) \vartheta(\mathbf{x}, s_0, t) = h(c) \nu(\mathbf{x}, t), \quad (21c)$$

$$\partial_t \eta(\mathbf{x}, t) + \nabla \cdot (\mathbf{u} \eta) = \mu_u(c) \nu(\mathbf{x}, t) + \int_{s_0}^{s^*} \mu_v(s, c) \vartheta(\mathbf{x}, s, t) ds, \quad (21d)$$

$$-D \nabla^2 c = f, \quad (21e)$$

with appropriate initial conditions and boundary condition on the spatial domains.

Integrating (21b) over s gives

$$\begin{aligned} \underbrace{\partial_t \left(\int_{s_0}^{s^*} \vartheta(\mathbf{x}, s, t) ds \right)}_{=-\partial_t \nu - \partial_t \eta} + g(s^*, c) \vartheta(\mathbf{x}, s^*, t) - \underbrace{g(s_0, c) \vartheta(\mathbf{x}, s_0, t)}_{=h\nu} \\ + \underbrace{\nabla \cdot \left(\mathbf{u} \int_{s_0}^{s^*} \vartheta(\mathbf{x}, s, t) ds \right)}_{=\nabla \cdot \mathbf{u}(1-\nu-\eta)} = - \int_{s_0}^{s^*} \mu_v(s, c) \vartheta(\mathbf{x}, s, t) ds. \end{aligned} \quad (22)$$

Substituting for $-\partial_t \nu - \partial_t \eta$ yields

$$\nabla \cdot \mathbf{u} = b(c) \nu. \quad (23)$$

Substituting $\mathbf{u} = -\lambda \nabla p$ gives an equation for the pressure in B_t ,

$$-\lambda \nabla^2 p = b(c) \nu. \quad (24)$$

Distributing the divergence operator gives

$$\nabla \cdot (\mathbf{u} \nu) = -\lambda \nabla p \cdot \nabla \nu + b(c) \nu^2, \quad (25a)$$

$$\nabla \cdot (\mathbf{u} \vartheta) = -\lambda \nabla p \cdot \nabla \vartheta + b(c) \nu \vartheta, \quad (25b)$$

$$\nabla \cdot (\mathbf{u} \eta) = -\lambda \nabla p \cdot \nabla \eta + b(c) \nu \eta. \quad (25c)$$

We see from (24) that p is proportional to λ^{-1} , so that $\lambda \nabla p$ is independent of λ . Consequently ν , ϑ , and η are independent of λ , allowing us to set $\lambda = 1$.

We impose periodic and other boundary conditions, similar to what was done in [1], to obtain the complete model. The active cell volume fractions satisfy

$$\begin{aligned} \partial_t \nu(\mathbf{x}, t) - \nabla p \cdot \nabla \nu &= -\mu_v(c)\nu(\mathbf{x}, t) + g(s^*, c)\vartheta(\mathbf{x}, s^*, t) \\ &\quad - h(c)\nu(\mathbf{x}, t) + b(c)\nu(\mathbf{x}, t)(1 - \nu(\mathbf{x}, t)), \end{aligned} \quad (26a)$$

for $x \in B_t$, $t > 0$ with conditions

$$\frac{\partial \nu}{\partial z} = 0, \quad \mathbf{x} \in \Gamma_B, t \geq 0, \quad (26b)$$

$$\nu(\mathbf{x}, 0) = \nu_0(\mathbf{x}), \quad \mathbf{x} \in B_t, \quad (26c)$$

where z denotes the spatial variable orthogonal to the surface Γ_B , and ν_0 is the initial active cell population. The dormant cell volume fractions satisfy

$$\begin{aligned} \partial_t \vartheta(\mathbf{x}, s, t) + \partial_s(g(s, c)\vartheta(\mathbf{x}, s, t)) - \nabla p \cdot \nabla \vartheta &= \\ &\quad - \mu_v(s, c)\vartheta(\mathbf{x}, s, t) - b(c)\nu(\mathbf{x}, t)\vartheta(\mathbf{x}, s, t), \end{aligned} \quad (26d)$$

for $x \in B_t$, $s > s_0, t > 0$, with conditions

$$g(s_0, c)\vartheta(\mathbf{x}, s_0, t) = h(c)\nu(\mathbf{x}, t), \quad \mathbf{x} \in B_t, t > 0, \quad (26e)$$

$$\frac{\partial \vartheta}{\partial z} = 0, \quad \mathbf{x} \in \Gamma_B, t \geq 0, s > s_0, \quad (26f)$$

$$\vartheta(\mathbf{x}, s, 0) = 0, \quad \mathbf{x} \in B_t, s \geq s_0. \quad (26g)$$

The fully inert cell volume fractions, including necrotic cells, satisfy

$$\begin{aligned} \partial_t \eta(\mathbf{x}, t) - \nabla p \cdot \nabla \eta &= \\ \mu_u(c)\nu(\mathbf{x}, t) + \int_{s_0}^{s^*} \mu_v(s, c)\vartheta(\mathbf{x}, s, t) ds - b(c)\nu(\mathbf{x}, t)\eta(\mathbf{x}, t), \end{aligned} \quad (26h)$$

for $x \in B_t$, $t > 0$, with conditions

$$\frac{\partial \eta}{\partial z} = 0, \quad \mathbf{x} \in \Gamma_B, t \geq 0, \quad (26i)$$

$$\eta(\mathbf{x}, 0) = \eta_0(\mathbf{x}), \quad \mathbf{x} \in B_t, \quad (26j)$$

where η_0 is the initial inert cell population. Pressure satisfies

$$-\nabla^2 p = b(c)\nu, \quad \mathbf{x} \in B_t, t \geq 0, \quad (26k)$$

$$p = 0, \quad \mathbf{x} \in \Gamma_t, t \geq 0, \quad (26l)$$

$$\frac{\partial p}{\partial z} = 0, \quad \mathbf{x} \in \Gamma_B, t \geq 0. \quad (26m)$$

Let $f = [f_1, \dots, f_m]$ and $c = [c_1, \dots, c_m]$. The chemical species satisfy, for $j = 1, \dots, m$,

$$-D_j \nabla^2 c_j = f_j, \quad \mathbf{x} \in \Omega, t > 0, \quad (26n)$$

$$f_j = 0, \quad \mathbf{x} \in \Omega \setminus B_t, \quad (26o)$$

$$c_j = c_j^*, \quad \mathbf{x} \in \Gamma_{H_b}, t \geq 0, \quad (26p)$$

$$\frac{\partial c_j}{\partial z} = 0, \quad \mathbf{x} \in \Gamma_B, t \geq 0, \quad (26q)$$

where the D_j are chemical diffusion coefficients and the c_j^* are the chemical concentrations in the bulk fluid. The normal velocity of the interface Γ_B is given by

$$-\nabla p \cdot \mathbf{n} = -\frac{\partial p}{\partial n}, \quad (26r)$$

where \mathbf{n} is the unit outward normal of Γ_B .

5 Computations

In this section we present computational results for models of batch cultures, chemostat cultures, and biofilms.

5.1 Batch Culture Dormancy As a Response to Nutrient Deprivation

We let $c(t)$ be a scalar value representing nutrient. We choose the functional forms

$$b(c) = \frac{kc}{\gamma + c}, \quad (27a)$$

$$h(c) = \frac{k_h}{\zeta + c} + \epsilon_h, \quad (27b)$$

$$g(s, c) = \frac{k_g c}{\gamma + c}, \quad (27c)$$

$$\mu_u(c) = \mu_u, \quad (27d)$$

$$\mu_v(s, c) = 0, \quad (27e)$$

$$f(c, u, v) = -\frac{kc}{Y(\gamma + c)} \left(u + \int_0^1 (e^{-s/k_g} + e^{-(1-s)/k_g}) v \, ds \right), \quad (27f)$$

$$v_0(s) = 0, \quad (27g)$$

with constant μ_u , rate constants k, k_h, k_g , saturation constant γ , Monod constant ζ , and yield constant Y . We take the baseline parameters $k = 1/4\text{hr}$, $\gamma = 4\text{g}_{\text{CODB}}/\text{m}^3$, $\epsilon_h = 0.05$, $\mu_u = 0.005/\text{hr}$, and $Y = 0.63\text{g}_{\text{CODB}}/\text{g}_{\text{CODS}}$ [19]. The units g_{CODB} and g_{CODS} are the chemical oxygen demand of biomass and substrate mass, resp. We assume a small ζ , say $\zeta = \gamma/20 = \text{g}_{\text{CODB}}/5\text{m}^3$. We

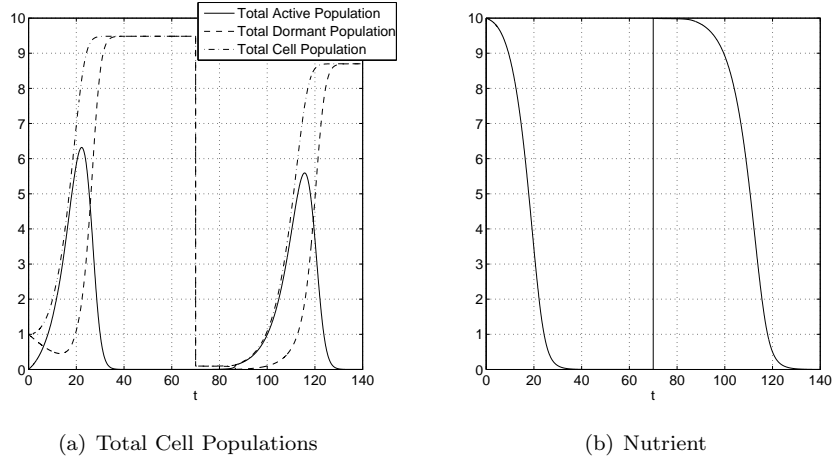


Figure 2: Results for the batch model, system (1) with $d_0 = 0$. We reculture 1% of each subpopulation into new media at $t = 70$ hours. Functional forms are as in (27) with parameters $k = 1/4\text{hr}$, $\gamma = 4\text{g}_{\text{CODB}}/\text{m}^3$, $\epsilon_h = 0.05$, $\mu_u = 0.005/\text{hr}$, $Y = 0.63\text{g}_{\text{CODB}}/\text{g}_{\text{CODS}}$, $\zeta = \text{g}_{\text{CODB}}/5\text{m}^3$, $k_h = \text{g}_{\text{CODB}}/(6\text{hr m}^3)$, and $k_g = 1/12\text{ hr}$. The dormancy domain is $[0, 1]$. Time is measured in hours.

require $k_h/\zeta \geq 1/24\text{hr}$, so take $k_h = \text{g}_{\text{CODB}}/(6\text{hr m}^3)$. We set the dormancy domain to be $s_0 = 0$ and $s^* = 1$, and assume 24 hr emergence at nutrient saturation so that $k_g = 1/12\text{ hr}$. As we reculture or restore nutrients, we see a reawakening of the population and a growth spurt until the new nutrient is also depleted. Results are shown in Figure 2 for reculturing of 1% of each subpopulation onto new substrate at $t = 70$ hours.

We conducted simulations with two species where 1% of each subpopulation was recultured into fresh media every 48, 72, and 168 hours. For shorter times of 4, 8, 16, and 24 (cases where 1% reculturing leads to extinction of all species), we used 100% reculturing. In all cases the fast-waker population ($k_g = 1/12\text{ hr}$) outgrew the slow-waker population ($k_g = 1/24\text{ hr}$). Although both active populations undergo oscillations, the fast-waker active population outgrows the slow-waker active population in each case. Moreover, the fast-waker total population dramatically outgrows the slow-waker total population in each case. (Results for 72-hour reculturing are shown in Figure 3.) This outcome is not surprising; conditions favor microbes that rapidly resuscitate.

5.2 Chemostat Culture Dormancy As a Response to Nutrient Deprivation

We use the functional forms and parameter values of Section 5.1, with $d_0 = k/2$ and $C_0(t) = 8 + 8\cos(\pi t/4)$. The active population, dormant population, and nutrient relax to a periodic oscillation. Results are shown in Figure 4.

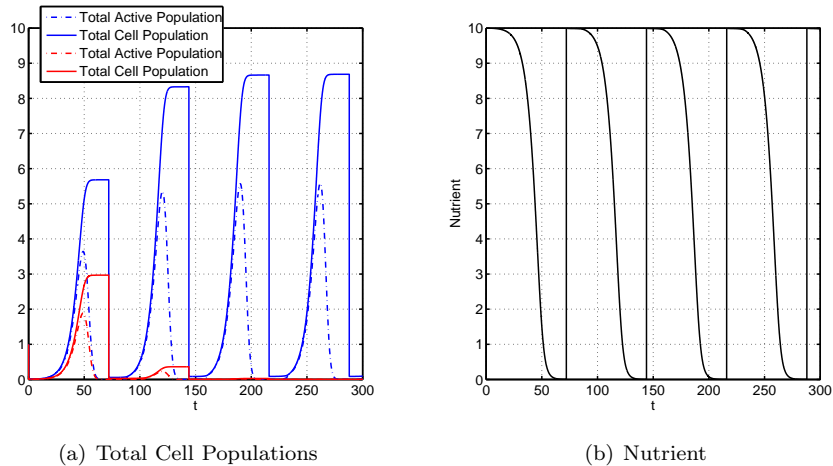


Figure 3: Results for the batch model for two species with $k_g = 1/12$ (blue) and $k_g = 1/24$ (red). We reculture 1% of each subpopulation into new media every 72 hours. All other parameters are as in Figure 2.

For two competing species, the only difference being $k_g = 1/12$ vs. $k_g = 1/24$, the results are shown in Figure 5. As in the batch case, the faster waker outcompetes the slower waker in the long run. This is true for a wide range of periods, $C(t) = 8 + 8 \cos(2\pi t p)$ with $p=0.5, 1, 4, 12, 24, 48, 72$ and 168 hours, verifying asymptotics predictions for short and long periods and extending to intermediate periods. Changes in period do not alter the numbers for a given subpopulation appreciably in magnitude, but rather change how they oscillate around some trajectory. The fast waker, as predicted, also outcompetes the slow waker in the case of a steady, rather than oscillating, nutrient source.

Computations of competing species in a chemostat, where one species undergoes no dormancy ($h = 0$) and the other undergoes dormancy with parameter $k_g = 1/12$, confirm the results of Section 3.2.1 (using $C(t) = 8 + 8 \cos(4\pi t)$ where t is measured in hours) and Section 3.2.2 (using $C(t) = 8 + 8 \cos(\pi t/4)$ where t is measured in hours). A species without dormancy capability will outcompete an otherwise similar species which can go dormant, under both fast and slow oscillations in nutrient.

5.3 Biofilm Dormancy as a Response to Nutrient Deprivation

In the biofilm model, (27f) becomes

$$f(c, \nu, \vartheta) = -\frac{k\rho^*c}{Y(\gamma + c)} \left(\nu + \int_0^1 (e^{-s/k_g} + e^{-(1-s)/k_g}) \vartheta ds \right). \quad (28)$$

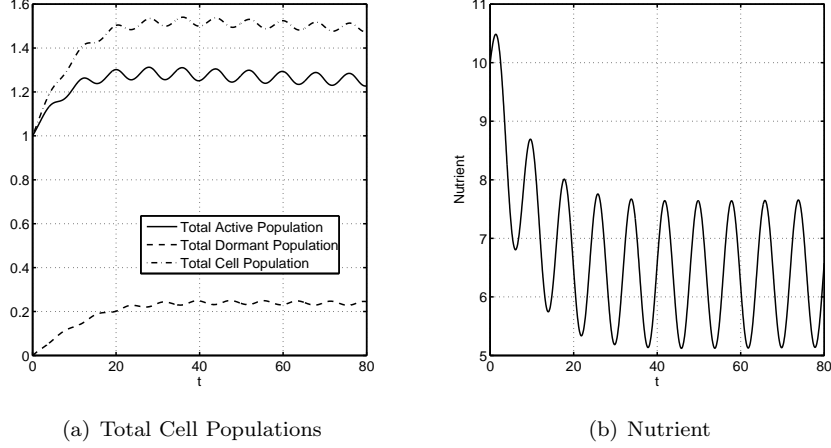


Figure 4: Results for the chemostat model, system (1) with $d_0 = k/2$ and $C(t) = 8 + 8 \cos(\pi t/4)$ where t is measured in hours. Functional forms are as in (27) with parameters $k = 1/4\text{hr}$, $\gamma = 4\text{g}_{\text{CODB}}/\text{m}^3$, $\epsilon_h = 0.05$, $\mu_u = 0.005/\text{hr}$, $Y = 0.63\text{g}_{\text{CODB}}/\text{g}_{\text{CODS}}$, $\zeta = \text{g}_{\text{CODB}}/5\text{m}^3$, $k_h = \text{g}_{\text{CODB}}/(6\text{hr m}^3)$, and $k_g = 1/12\text{ hr}$. The dormancy domain is $[0, 1]$. Time is measured in hours.

We use the functional forms and parameter values of Section 5.1, with the addition of $\rho^* = 10^4\text{g}_{\text{CODB}}/\text{m}^3$ and $D = 10^{-4}\text{m}^2/\text{day}$ [19].

Results shown in Figure 6 indicate that the slow waker has comparable total live biomass than the fast waker, and possibly more in lower regions, and palpably more dormant biomass, even though the faster wakers outnumber the slower wakers near the top of the biofilm.

6 Computational Methodology

As was done for senescence-structure in [5, 12], we often handle a general physiologically structured system such as (1a)-(1c) more easily if it is transformed to an age-structured system, whether in the statement of the problem, or indirectly in the numerical method [9]. Let $a \geq 0$ represent time a cell has spent dormant. We make a change of variables so that dormancy, $s(a, t)$, is a separate function of age and time. We then get age-structured equations for v ,

$$\partial_t v(a, t) + \partial_a v(a, t) = -\tilde{\mu}_v(s, c)v(a, t) - Dv(a, t), \quad 0 < a \leq a^*, t > 0, \quad (29a)$$

$$v(0, t) = h(c)u(t), \quad t > 0, \quad (29b)$$

$$\partial_t s(a, t) + \partial_a s(a, t) = g(s(a, t), c(t)), \quad 0 < a \leq a^*, t > a, \quad (29c)$$

$$s(0, t) = s_0, \quad (29d)$$

where $\tilde{\mu}_v(s, c) = \mu_v(s, c) + \partial_s g(s, c)$ and $s(a^*, t) = s^*$. The condition (27g) means we need only consider $t > a$ for the domain of $s(a, t)$.

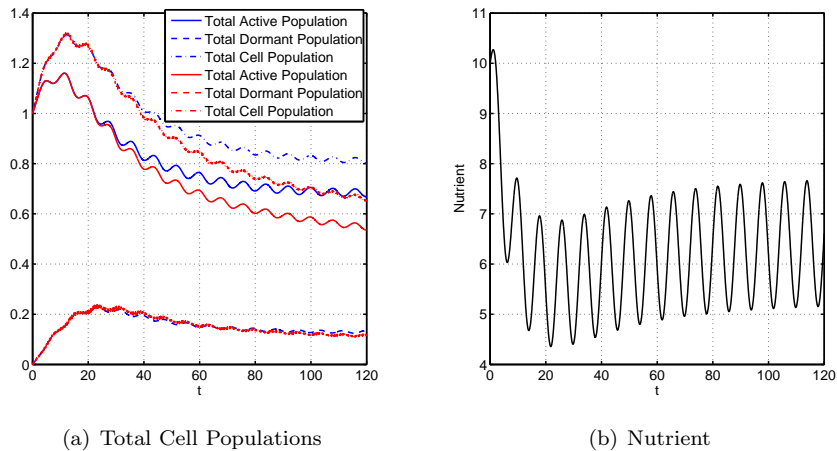


Figure 5: Results for the chemostat model for two species with $k_g = 1/12$ (blue) and $k_g = 1/24$ (red). All other parameters are as in Figure 4. In the long run, the slow waker is driven to extinction.

For our choice, $g(s, c) = \frac{k_g c}{\gamma_g + c}$ for scalar c , we get

$$s^* = s_0 + \int_{t-a}^t \frac{\gamma_g + c(\tau)}{k_g c(\tau)} s^* d\tau, \quad (30)$$

so that $a^* \rightarrow \infty$ if $c \rightarrow 0$. Since functions with similar behavior to g are natural representations of the dormancy dynamics, we find that the original physiologically structured system is more tractable computationally than the equivalent age-structured system for most forms of g that interest us.

To solve equations with more general physiological structure, we use an extension of the natural-age-grid Galerkin methods developed for age- and space-structured systems in [2, 3]. These methods move the discretization nodes in age smoothly along characteristic lines. The solutions are approximated by piecewise polynomials, rather than moments as was done by de Roos [8]. Our extension of our methods to general physiological structure moves the discretization nodes in the physiological variable along characteristic curves, similar to a method of Sulsky [18], but with the preservation of the property in our methods that each time step need not result in a new discretization node in the physiological variable. This is essential when variation of spatial structure, or any other dynamics in the problem, occurs on a faster time scale than that of the physiological trait. Otherwise, the need to take lots of small time steps would induce many more physiological nodes than are necessary for accuracy, resulting in potentially great loss of efficiency from additional computation or interpolation onto a coarser grid.

To motivate the integration in age and time, we ignore for the moment the discretization in space. We partition the domain $[s_0, s^*]$ at each time by the set

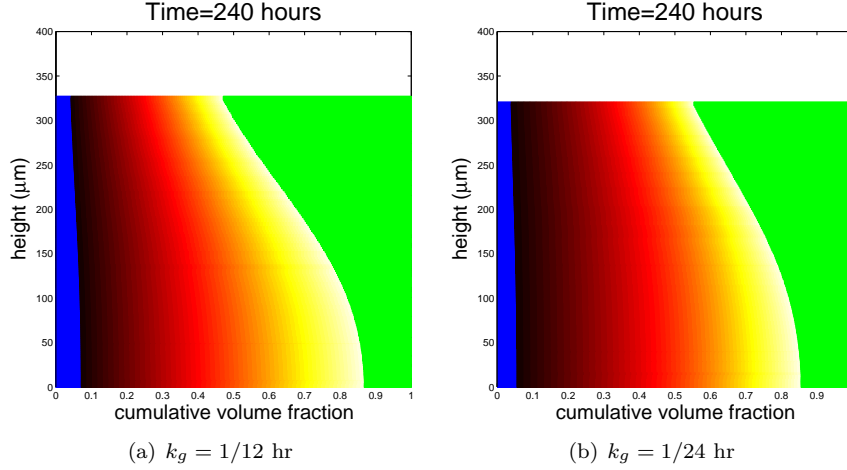


Figure 6: Results for the biofilm model, system (26). Functional forms are as in (27) except that f given by (28). Parameters $k = 1/4$ hr, $\gamma = 4g_{\text{CODB}}/\text{m}^3$, $\epsilon_h = 0.05$, $\mu_u = 0.005/\text{hr}$, $Y = 0.63g_{\text{CODB}}/g_{\text{CODS}}$, $\zeta = g_{\text{CODB}}/5\text{m}^3$, $k_h = g_{\text{CODB}}/(6\text{hr m}^3)$. The two figures differ in the values of k_g . The dormancy domain is $[0, 1]$. Time is measured in hours. The horizontal width of a color constitutes the volume fraction of cells of in the corresponding state. Green denotes active cells, blue denotes fully inert cells, and the “hot” black-red-yellow-white spectrum denotes dormancy from 0 to 1. While fast reactivators are more prevalent near the top of the biofilm, slow reactivators have more biomass, particularly in dormant (hence resistant) form, in deeper biofilm layers.

of nodes $\{s_i(t)\}_{i=0}^N$ where $s_0(t) = s_0$. If $s_N(t) \geq s^*$, we simply ignore that node and the function value over it until needed. This is not an issue for our choices of g . We compute the solution at times t_j and let $\Delta t_j = t_{j+1} - t_j$, $s_{i,j} = s_i(t_j)$, and $\Delta s_{i,j} = s_{i+1,j} - s_{i,j}$. For the last interval we use $\Delta s_{N,j} = \max(s^* - s_{N,j}, 0)$. Although we are not including space in this discussion for reasons of clarity, the presence of spatial structure in a problem will induce different time scales into a problem, making adaptivity and nonuniformity of time intervals an important property of any method used.

For the computations in this paper, we use a piecewise constant approximation space over the domain $[s_0, s^*]$. Higher-order approximation spaces can be used, as was done in age in [2]. We define the projection into the space of piecewise constants over the partition of $[s_0, s^*]$ by

$$\Pi(v(s, t_j)) = \begin{cases} \frac{1}{\Delta s_{i,j}} \int_{s_{i,j}}^{s_{i+1,j}} v(s, t_j) ds, & \text{if } s_{i,j} \leq s < s_{i+1,j}, \\ 0, & \text{otherwise.} \end{cases} \quad (31)$$

We make the approximation $V_{i,j} \approx \Pi(v(s, t_j))$ via the following algorithm. Let Δs_{max} be the largest we want the first interval in s to be. For most time

steps we have $\Delta s_{0,j} \leq \Delta s_{\max}$. In this case we set

$$s_{i,j+1} = s_{i,j} + \Delta t_j g(s_{i,j}, c(t_j)), \quad \text{for } i = 1, \dots, N. \quad (32a)$$

We choose Δt_j such that $s_{i,j+1} \geq s^*$ for at most one i , so as to keep N fixed.

Let the value $V_{i,j}$ denote the density over $[s_{i,j}, s_{i+1,j}]$ for $i = 1, \dots, N-1$. We use $\mathcal{B}(t)$ to denote the creation of newly dormant cells at s_0 . Then

$$V_{i,j+1} = \frac{\Delta s_{i,j}}{\Delta s_{i,j+1}} V_{i,j}, \quad \text{for } i = 1, \dots, N-1, \quad (32b)$$

$$V_{0,j+1} = \frac{1}{\Delta s_{0,j+1}} (\Delta s_{0,j} V_{0,j} + \Delta t_j \mathcal{B}(t_j)), \quad (32c)$$

$$V_{N,j+1} = \frac{\Delta s_{N-1,j} - \Delta t_j}{\Delta s_{N,j+1}} V_{N-1,j}. \quad (32d)$$

Because the applications in this paper provide for the first extension of the methods presented in [2, 3], we have kept $\mathcal{B}(t)$ general in this part of the presentation of the method. In our case we have $\mathcal{B}(t_j) = g(s_0, c(t))v(s_0, t)$. Also, if g is independent of s , we have $\Delta s_{i,j}/\Delta s_{i,j+1} = 1$ for $i = 1, \dots, N-1$.

If $\Delta s_{0,j} > \Delta s_{\max}$, we introduce a new node and set

$$s_{i+1,j+1} = s_{i,j} + \Delta t_j g(s_{i,j}, c(t_j)), \quad \text{for } i = 1, \dots, N-1, \quad (32e)$$

$$V_{i+1,j+1} = \frac{\Delta s_{i,j}}{\Delta s_{i,j+1}} V_{i,j}, \quad \text{for } i = 0, \dots, N-1, \quad (32f)$$

for the intermediate intervals, and set

$$s_{1,j+1} = \Delta t_j g(s_0, c(t_j)), \quad (32g)$$

$$V_{0,j+1} = \frac{\Delta t_j \mathcal{B}(t)}{\Delta s_{0,j+1}}, \quad (32h)$$

$$V_{N,j+1} = \frac{\Delta s_{N-1,j} V_{N-1,j} + (\Delta s_{N,j} - \Delta t_j g(s^*, c(t_j))) V_{N,j}}{\Delta s_{N,j+1}}, \quad (32i)$$

for the first and last intervals.

The above calculations account for transport in the physiological variable, entry into dormancy, and exit from dormancy. Upwind differences approximate the advection terms in space. Center differences approximate the diffusion terms in space. Backward Euler formulæ, embedded in step-doubling with local extrapolation, approximate the time derivatives. This creates a likely second-order correct time integration scheme [4].

7 Conclusions

Modeling results suggest that spatial heterogeneity in biofilms can support a rich dormancy structure. For example, whereas dormant cells near the top of

a biofilm would need to be able to resuscitate quickly (small s^* , large g) when environmental conditions improve in order to be competitive, dormant cells lower in the biofilm, where the slower waker has a defensive advantage over the fast waker due to a larger amount of dormant biomass without an appreciable difference in total live biomass, may be able to afford to be more cautious (large s^* , small g).

In contrast, dormancy-capable cells in well-mixed, planktonic systems (e.g. batch and chemostat cultures) appear to have less advantage over “regular” cells. In the absence of spatially structured populations, live biomass is maximized by the fastest possible exit from dormancy. The lower limit of time to reawakening is governed by physiological, biochemical or other constraints within the cells, and hence dormancy mechanisms are constrained to easily reversible mechanisms. As most lab populations are of the well-mixed batch or chemostat sort, and most natural populations are of the spatially-structured biofilm sort, this presents a possible drawback in use of typical laboratory systems for characterization of natural ones.

We remark that we have only considered here dormancy response in the context of resource deprivation. Dormancy is also likely an effective defense strategy against antimicrobial agents – many antimicrobials are only effective against metabolically active targets. Thus the presence of antimicrobials reinforces the utility of dormancy in biofilms and also may advantage dormancy-capable populations in well-mixed cultures. The nature of dormancy as defense could itself benefit from modeling studies.

More generally, beyond dormancy specifically, recent studies suggest that phenotypic heterogeneity of many sorts is typical in spatially structured microbial populations such as biofilms [6]. Hence, methods of the sort presented here are likely to be useful and possibly necessary for modeling the function and ecology of spatially unmixed microbial populations of the sort that dominate the natural environment.

Acknowledgments

The authors thank Phil Stewart for helpful ideas and discussions.

References

- [1] Erik Alpkvist and Isaac Klapper. A multidimensional multispecies continuum model for heterogeneous biofilm development. *Bull. Math. Biol.*, 69(2):765–789, 2007.
- [2] Bruce P. Ayati. A variable time step method for an age-dependent population model with nonlinear diffusion. *SIAM J. Numer. Anal.*, 37(5):1571–1589, 2000.

- [3] Bruce P. Ayati and Todd F. Dupont. Galerkin methods in age and space for a population model with nonlinear diffusion. *SIAM J. Numer. Anal.*, 40(3):1064–1076, 2002.
- [4] Bruce P. Ayati and Todd F. Dupont. Convergence of a step-doubling Galerkin method for parabolic problems. *Math. Comp.*, 74(251):1053–1065, July 2005.
- [5] Bruce P. Ayati and Isaac Klapper. A multiscale model of biofilm as a senescence-structured fluid. *Multiscale Model. Simul.*, 6(2):347–365, 2007.
- [6] Blaise R. Boles, Matthew Thoendel, and Pradeep K. Singh. Self-generated diversity produces “insurance effects” in biofilm communities. *PNAS*, 101(47):16630–16635, 2004.
- [7] Luis E. Chávez de Paz, Ian R. Hamilton, and Gunnel Svensäter. Oral bacteria in biofilms exhibit slow reactivation from nutrient deprivation. *Microbiology*, 154:1927–1938, 2008.
- [8] A. M. de Roos. Numerical methods for structured population models: The escalator boxcar train. *Num. Meth. Part. Diff. Eqns.*, 4:173–195, 1989.
- [9] A. M. de Roos. A gentle introduction to physiologically structured population models. In S. Tuljapurkar and H. Caswell, editors, *Structured-population Models in Marine, Terrestrial, and Freshwater Systems*, volume 18 of *Population and Community Biology Series*, chapter 5, pages 119–204. Chapman & Hall, New York, 1997.
- [10] J. Dockery and I. Klapper. Finger formation in biofilm layers. *SIAM J. Appl. Math.*, 62(3):853–869, 2001.
- [11] Isaac Klapper and Jack Dockery. Mathematical description of microbial biofilms. *SIAM Rev*, 52(2):221–265, 2010.
- [12] Isaac Klapper, Peter Gilbert, Bruce P. Ayati, Jack Dockery, and Philip Stewart. Senescence can explain microbial persistence. *Microbiology*, 153(11):3623–3630, 2007.
- [13] Tufail Malik and Hal Smith. A resource-based model of microbial quiescence. *J. Math. Biol.*, 53(2):231–252, 2006.
- [14] Tufail Malik and Hal L Smith. Does dormancy increase fitness of bacterial populations in time-varying environments? *Bull. Math. Biol.*, 70(4):1140–1162, 2008.
- [15] Johanna Roostalu, Arvi Jõers, Hannes Luidalepp, Niilo Kaldalu, and Tanel Tenson. Cell division in *Escherichia coli* cultures monitored at single cell resolution. *BMC Microbiology*, 8(68):1–14, 2008.

- [16] Hal L. Smith and Paul Waltman. *The Theory of the Chemostat*. Number 13 in Cambridge Series in Mathematical Biology. Cambridge University Press, 1995.
- [17] Philip S. Stewart and Michael J. Franklin. Physiological heterogeneity in biofilms. *Nature Reviews Microbiology*, 6(3):199–210, 2008.
- [18] Deborah Sulsky. Numerical solution of structured population models, II. mass structure. *J. Math. Biol.*, 32:491–514, 1994.
- [19] Oskar Wanner, Hermann Eberl, Eberhard Morgenroth, Daniel Noguera, Cristian Picioreanu, Bruce Rittmann, and Mark Van Loosdrecht. *Mathematical Modeling of Biofilms*. Number 18 in IWA Scientific and Technical Reports. IWA Publishing, London, 2006.
- [20] T. C. Zhang, Y. C. Fu, and P. L. Bishop. Competition in biofilms. *Wat. Sci. Tech.*, 29(10-11):263–270, 1994.

